Towards understanding respiratory particle transport and deposition in the human respiratory system: Effects of physiological conditions and particle properties

Zhiyi Yao[1], Tianyang Zhao[2], Weiling Su[1], Siming You[2,3], Chi-Hwa Wang[1*]

1. Department of Chemical and Biomolecular Engineering, National University of Singapore, 4 Engineering Drive 4, Singapore 117585
2. NUS Environmental Research Institute, National University of Singapore, 1 Create Way, Create Tower, #15-02, Singapore 138602
3. James Watt South Building, School of Engineering, University of Glasgow, G12 8QQ

*Corresponding Author. Tel: +65 65165079;

Email: chewch@nus.edu.sg (C. H. Wang)

Submitted for Publication to

Journal of Hazardous Materials

July 2022

Abstract:

Fly ash is a common solid residue of incineration plants and poses a great environmental concern because of its toxicity upon inhalation exposure. The inhalation health impacts of fly ash is closely related to its transport and deposition in the human respiratory system which warrants significant research for health guideline setting and inhalation exposure protection. In this study, a series of fly ash transport and deposition experiments have been carried out in a bifurcation airway model by optical aerosol sampling analysis. Three types of fly ash samples of different morphologies were tested and their respiratory deposition and transport processes were compared. The deposition efficiencies were calculated and relevant transport dynamics mechanisms were discussed. The influences of physiological conditions such as breathing rate, duration, and fly ash physical properties (size, morphology, and specific surface area) were investigated. The deposition characteristics of respiratory particles containing SARS-CoV-2 has also been analyzed, which could further provide some guidance on COVID-19 prevention. The results could potentially serve as a basis for setting health guidelines and recommending personal respiratory protective equipment for fly ash handlers and people who are in the high exposure risk environment for COVID-19 transmission.

Keywords: Fly ash; Deposition; Respiration; Toxicology; COVID-19.

Environmental Implication

Fly ash is a common solid residue produced from incineration plants and it poses a great environmental concern because of its toxicity upon inhalation exposure. Fly ash can cause high carcinogenic risks, and increase the risks of cardiovascular morbidity. The inhalation health impacts of fly ash are closely related to its transport and deposition in the human respiratory system. We have conducted a series of fly ash transport experiments to investigate its deposition characteristics in human respiratory system. The results could serve as a basis for setting health guidelines and recommending personal respiratory protective equipment for fly ash handlers.

1 Introduction

Fly ash is a common solid residue produced from the combustion of fossil fuels and waste. Over 600 million tons of fly ash is produced globally every year and this number is expected to increase substantially in the face of the increasing demand in energy and waste disposal (Nyale et al., 2013; Terzić et al., 2015). This massive fly ash production poses an environmental concern as fly ash threatens human health upon inhalation exposure (Johnson, 2016; Sgro et al., 2012). Recent studies showed that fly ash particles were generally polydispersed and enriched in various harmful compositions such as heavy and transition metals, polycyclic aromatic hydrocarbons (PAHs), organochlorines, polychlorinated dibenzo-p-dioxins, and polychlorinated dibenzofurans (Carvalho et al., 2014; Li et al., 2017; Santa et al., 2016; Wu et al., 2016). Even a low-dose exposure to fly ash was able to induce adverse changes in pulmonary mechanics, cause high carcinogenic risks, and increase the risks of cardiovascular morbidity and mortality (Carvalho et al., 2014; Marchini et al., 2014; Wu et al., 2016). Furthermore, fly ash nanoparticles are a particular health concern because of its relatively large surface area and harmful compositions which could produce oxidative stress, exert genotoxic effects, and translocate to other targets such as the cardiovascular system, spleen and liver (Dwivedi et al., 2012; Matzenbacher et al., 2017; Oliveira et al., 2017). Particle transport and deposition in the human respiratory system are closely related to the health impacts of particulate inhalation exposure (Fang et al., 2017; You et al., 2017). It is also important to understand the mechanisms governing the respiratory transport and deposition phenomena which lays the foundation for developing effective measures for inhalation exposure protection. The human respiratory system could be divided into three major regions, *i.e.* the extrathoracic (ET) region (from the nose to trachea), tracheobronchial region (TB) (from the trachea to bronchi), and the alveolar region (Megido et al., 2016; Zhang et al., 2006). The dimensions of the regions vary considerably from person to person and the morphology of the system becomes increasingly sophisticated deeply into the alveolar region, but it is generally acceptable to simplify the airways of the TB and alveolar regions as a system of symmetrically branching tubes with decreasing diameters for mechanistic studies (Peslin and Fredberg, 2011). In this case, a bipodial geometry could be assumed for the airway tree where the parent airway branches into two daughter airways at each bifurcation with the trachea being the root (zero generation) of the airway tree (Aykac et al., 2003; Banko et al., 2015). (Kim and Fisher, 1999) showed that there was only a slight difference between two successive bifurcations, suggesting that the data from a single bifurcation model is representative. Actually, it is prohibitive to cover all the regions in modelling and experimental works on human respiratory deposition due to the sophistication of the respiratory system. Bifurcation models, in this case, serve as an efficient means to explore the fundamental aerosol and fluid dynamics underlying the transport and deposition processes.

Both experimental and modelling studies have been conducted to explore the particle deposition in the human respiratory system based on bifurcation airway models. For example, in early studies, the flow patterns in two successive generations of bronchial tree were investigated using flow visualization methods and hot-wire anemometers (Bharadvaj et al., 1982). Subsequently, due to the relatively high accuracy and nonintrusiveness of laser-Doppler velocimetry, it was applied to bifurcation airway models with a higher number of branching (Jedelsky et al., 2012; Kerekes et al., 2016; Theunissen and Riethmuller, 2007). (Xu et al., 2009) explored the effects of oscillatory flow on the deposition pattern of aerosol particles in a single bifurcation tube using a laser-photodiode measurement technique. Recently, aerosol deposition in the respiratory system was also investigated by high-speed photography techniques that bear the advantages of being straightforward and low-cost (Goikoetxea et al., 2014; Tong et al., 2016). Simulation was also used to understand the trajectories of aerosol particles in respiratory airways with a special focus on the effects of particle size, flow rate, and flow profile on the spatial deposition patterns of particles (Feng and Kleinstreuer, 2014; Kolanjiyil and Kleinstreuer, 2016; Rahimi-Gorji et al., 2016). Empirical mathematical models of respiratory deposition have been proposed based on experimental or simulation data (e.g., (Park and Wexler, 2008; Shanley et al., 2016; Zamankhan et al., 2006)). These models were generally limited to a given respiratory region and particle size range (e.g., nanoparticles and microparticles). These existing studies are generally featured by the assumption or utilization of spherical particles, which means that relevant findings and models are not necessarily applicable for the case of fly ash that are irregular in terms of morphology.

Coronavirus disease 2019 (COVID-19) is an infectious disease caused by severe acute respiratory syndrome coronavirus 2 (SARS-CoV-2) (Coronaviridae Study Group of the International Committee on Taxonomy of, 2020), and nowadays our lives are still severely affected by it. It was reported that as of February 24, 2022, there have been more than 430 million cases of COVID-19 infection worldwide, including more than 5.93 million death cases (worldometer, 2022). Several studies observed the correlation between the levels of lethality of SARS-CoV-2 and atmospheric pollution. It was suggested that particulate pollution may be possible co-factor of COVID-19 (Conticini et al., 2020; **J. Marvin Herndon**, 2020). It was reported that fly ash contained many pores which might carry virus to human airways (Bao et al., 2015). If the upper respiratory tract is infected by the SARS-CoV-2, common symptoms include rhinitis and sore throat. In contrast, when the lower respiratory tract gets infected, more severe symptoms could be caused, such as pneumonia, bronchitis, and bronchiolitis (Subbarao and Mahanty, 2020). SARS-CoV-2 could be transmitted from person to person through respiratory particles (RPs) such as droplets and aerosols (Jayaweera et al., 2020). Aerosols are divided into natural aerosols and anthropogenic aerosols. Fly ash is one of the anthropogenic aerosols (Hidy, 2012). SARS-CoV-2 primarily attacks human lung airways, ultimately impairing the gas exchange capacity of the lungs (Mason, 2020). Therefore, it is important to study the deposition of respiroatory particles containing SARS-CoV-2 virus in lung. Particle deposition in the lungs is related to the physics of the particles, the anatomy of the respiratory tract, and the airway pattern in the lung airways (Sankhala et al., 2013). RPs have a broad range of sizes ranging from less than 1 μm to 10 μm (Lee et al., 2019). These RPs are approximately spherical in the air. The spike(s) protein, one of the structural proteins on SARS-CoV-2, binds to the host cell surface receptor angiotensin-converting enzyme 2 (ACE2) via the receptor binding domain (RBD) (Yao et al., 2020). In addition to binding to ACE2, the amount of virus deposited on the receptor also plays an important role in viral infection. There are a lot of studies that have been conducted to investigate the deposition of SARS-CoV-2 in human airways using the stochastic lung deposition model and compositional fluid dynamics (CFD) (Islam et al., 2021; Madas et al., 2020; Wedel et al., 2021). However, there is still a lack of experimental study that validates the theoretical models.

In this work, we conducted a series of fly ash transport and deposition experiments in a bifurcation airway model using optical aerosol sampling analysis. The deposition efficiencies were calculated and relevant transport dynamics mechanisms were discussed. Three types of fly ash particles of different morphologies were tested, and their respiratory deposition processes were compared. The influences of physiological conditions and the physical properties of fly ash particles were investigated. Since the size and the feature of respiratory particles that SARS-CoV-2 is attached to are similar to the fly ash of spherical shape, the deposition percentage (DP) of respiratory particles containing SARS-CoV-2 has also been investigated in this study. The effects of RP size and breathing conditions on DP in the airway were investigated and discussed, which could further provide some guidance on COVID-19 prevention. The results could serve as a basis for setting health guidelines and recommending personal respiratory protective equipment for fly ash handlers and people who are in the high exposure risk environment for COVID-19 transmission.

2 Methodology

2.1 Fly Ash

Three types of fly ash samples were collected on-site from local industrial incinerators. Fly ash a, fly ash b and fly ash c was produced from combustion of coal, combustion of biomass, and combustion of sewage sludge, respectively. Their morphology and surface properties were characterized using scanning electron microscopy (SEM) and Brunauer–Emmett–Teller (BET) tests, respectively. For SEM imaging, each sample was dried overnight, then evenly spread on a conductive (carbon) double-sided tape and mounted on a specimen stub. The particles were sputtered with a thin-layer of metal (Pd & Pt) under a low vacuum condition prior to the SEM analysis (Hong et al., 2017). The BET theory assumed that inert gas molecules would adsorb onto particle surfaces forming infinite layers and the Langmuir theory was applied to calculate the specific surface area.

2.2 Experiments

2.2.1 Experimental setup

The schematic diagram of experimental setup is shown in **Fig. 1**. An aerosol generator (Palas GmbH, RGB 1000G) was used to dispense (one-off) fly ash into aerosol chamber 1 (immediately before the bifurcation model) before the flowing system was switched on. The particle number concentration (C_1) in the chamber was recorded using an aerosol spectrometer (GRIMM 1.109) in real-time. Valves, a vacuum pump, and a logical controller (Mitsubishi Al-10MR-A) were used to simulate a continuous oscillatory flow in the human respiratory system including separate inhalation and exhalation cycles (typically 2 to 4 seconds). The logic controller was used to automate the swinging process between the inhalation and exhalation cycles at pre-set durations. Another aerosol spectrometer was used to measure the real-time particle number concentration (C_2) in aerosol chamber 2 immediately after the left lobe of the bifurcation model. A third chamber is immediately after the right lobe and used to alleviate the effects of aerosol chambers on the symmetry of the system. All the chambers have the same volume of V. For exhalation, the air is withdrawn from the fume hood through the bifurcation tube into the atmosphere.

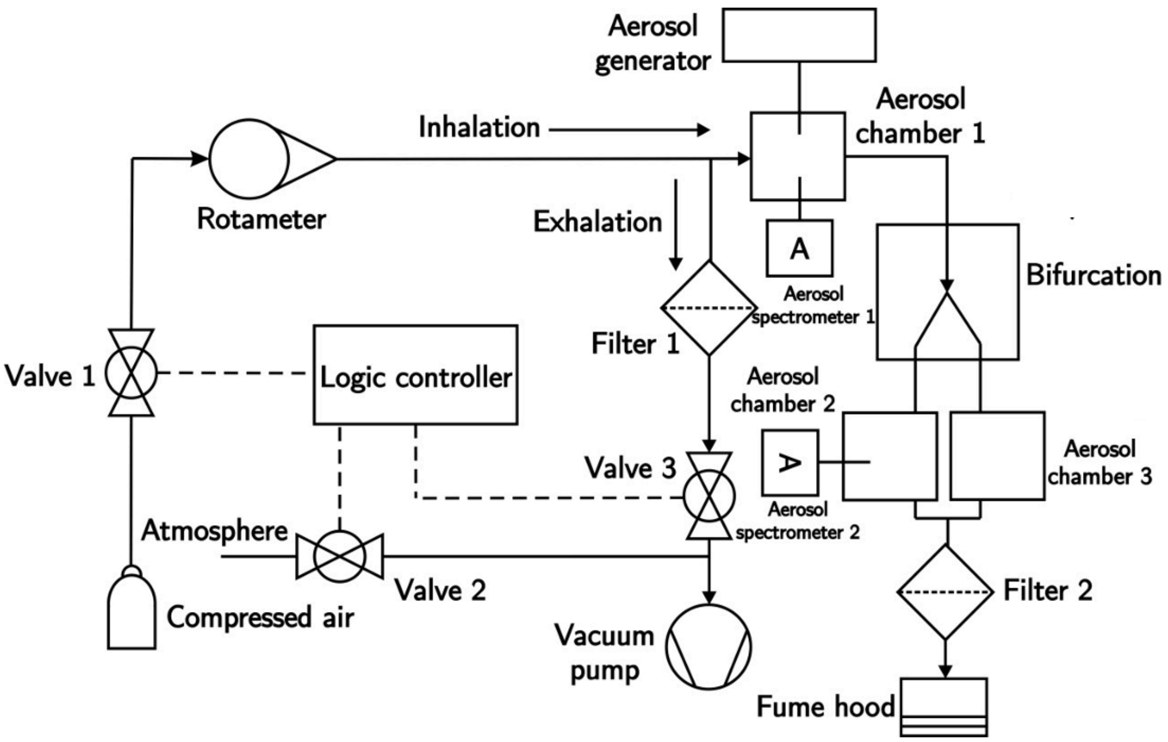

Fig. 1. A schematic diagram of experimental setup.

The bifurcation model consists of a single quartz bifurcation tube branching out to two daughter tubes, mimicking that of the trachea to two main bronchi airways. The inner diameters of the parent tube and daughter tubes are 1.6 and 0.8 cm, respectively while the mouth of the parent tube and the tails of the daughter tubes are 1.0 and 0.4 cm, respectively. The trachea of a normal adult generally has a diameter between 1 and 2 cm and its subsequent three generations (bronchioles) typical have a diameter range between 0.1 and 0.5 cm (Aykac et al., 2003). In general, the length of trachea ranges from 5.8 to 9.2 cm while the length of bronchus ranges from 1.6 to 4.5 cm (Shaik et al., 2017). The lengths of the parent and daughter tubes are 8.5 and 7.5 cm, respectively.

2.2.2 Experimental arrangement

The respiratory rate for adults ranges from 12 rpm under rest condition to 35 rpm under stress test condition. The minute ventilation rate of adults is between 6 L/min and 105 L/min (Pleil et al., 2021). In this study, the influences of three physiological factors, i.e. breathing rate (10 and 25 L/min), duration (2, 3 and 4 seconds), towards the transport and deposition of fly ash particles were investigated. The case of lower breathing rate and longer duration corresponds to that of a resting person, while the case of higher breathing rate and shorter duration correspond to that of an exercising person. Each experimental case was repeated for three times for statistical analysis and each run lasts for one minute.

2.3 Deposition efficiency and deposition percentage

The deposition efficiency (DE) is defined as the fraction of fly ash particles deposited onto the surface of the airway model in an inhalation or expiration cycle. Particle deposition occurs during both inhalation (DE_1) and expiration (DE_2) cycles. We employed mass balance models to backward calculate the deposition efficiencies based on temporal variation of airborne fly ash concentrations in chamber 1 and 2 under the assumption that DE_1 and DE_2 are contants. For an inhalation cycle, the fly ash particle concentrations in the first and second chambers are analysed in the following way:

Chamber 1 from inhalation to exhalation chamber: n-1 to n

$$V_1 C_{1,n} = V_1 C_{1,n-1} - DE_1 V_1 C_{1,n-1} + \left(C_\infty - C_{1,n-1}\right)\dot{V}dt + Sdt \quad (1)$$

Where V_1 (m^3) is the volume of chamber 1. $C_{1,n}$ ($\#/m^3$) refers to the particle concentration in chamber 1 in the n^{th} cycle. $C_{1,n-1}$ ($\#/m^3$) refers to the particle concentration in chamber 1 in the (n-1)th cycle. DE_1 is the deposition efficiency of ash particle in chamber 1. C_∞ (#/m^3) is the particle concentration in the environment. $\dot{V}$ (m^3/s) is the ventilation rate, S [#/(m^{3}s)] refers to the generation rate of the ash from aerosol generator. In contrast, from exhalation to inhalation chamber: n to n+1

$$V_1 C_{1,n+1} = V_1 C_{1,n} - DE_1 V_1 C_{1,n} + \left(C_{2,n} - C_{1,n}\right)\dot{V} dt + S dt \qquad (2)$$

Where $C_{1,n+1}$(#/m^3) refers to the particle concentration in chamber 1 in the (n+1)th cycle.

Chamber 2 from inhalation to exhalation chamber: n-1 to n

$$V_2 C_{2,n} = V_2 C_{2,n-1} - DE_2 C_{2,n-1} + \left(C_{1,n} - C_{2,n}\right)\frac{\dot{V}}{2} dt \qquad (3)$$

Where V_2 (m^3) is the volume of chamber 2. $C_{2,n}$ (#/m^3) refers to the particle concentration in chamber 2 in the nth cycle. $C_{2,n-1}$ (#/m^3) refers to the particle concentration in chamber 2 in the (n-1)th cycle. DE_2 is the deposition efficiency of ash particle in chamber 2.

In contrast, from exhalation to inhalation chamber: n to n+1

$$V_2 C_{2,n+1} = V_2 C_{2,n} - DE_2 V_2 C_{2,n} + \left(C_\infty - C_{2,n}\right)\frac{\dot{V}}{2} dt \qquad (4)$$

Where $C_{2,n+1}$ (#/m^3) refers to the particle concentration in chamber 2 in the (n+1)th cycle.

Solving equations (1) & (2), DE_1 can be obtained using the following equation:

$$DE_1 = \left\{ \frac{\left[\frac{\dot{V}}{V_1}\left(C_{2,n} - C_\infty\right) - \frac{C_{1,n+1} - 2C_{1,n} + C_{1,n-1}}{dt}\right]}{C_{1,n} - C_{1,n-1}} - \frac{\dot{V}}{V_1} \right\} dt \qquad (5)$$

Solving equations (3) & (4), DE_2 can be obtained using the following equation:

$$DE_2 = \left\{ \frac{\left[\frac{\dot{V}}{2V_2}\left(C_\infty - C_{1,n-1}\right) - \frac{C_{2,n+1} - 2C_{2,n} + C_{2,n-1}}{dt}\right]}{\left(C_{2,n} - C_{2,n-1}\right)} - \frac{\dot{V}}{2V_2} \right\} dt \qquad (6)$$

Since the breathing duration is smaller than the sampling interval of the aerosol spectrometers (6 seconds), the deposition efficiencies (DE_1 and DE_2) were estimated by fitting Eq. (3), Eq. (4), Eq. (5), and Eq. (6) to the temporal concentration data of five cycles. Particle deposition in the chambers is assumed to be negligible because it is significantly smaller than the effect of ventilation and correspond to a short period of time (< 25 seconds).

Deposition percentage (DP) in each tube is defined as the ratio of the number of deposited particles and the total number of particles that are inhaled.

In chamber 1, the DP is calculated as:

$$DP_1 = DE_1 \quad (7)$$

In chamber 2, the DP is calculated as:

$$DP_2 = (1 - DE_1)DE_2 \quad (8)$$

2.4 Health risk assessment (HRA)

The cell-based and in vivo toxicity of ash have been reported in our group's previous publications. Mozhi et. Al. have analyzed toxicity effects of both solid ash and ash leachate on human lung fibroblast cells (MRC-5) and human skin epidermal cells (HaCaT) (Mozhi et al., 2022). Direct contact with both solid ash and ash leachate was found to result in the cell membrane leakage, destructive mitochondrial membrane potential, apoptosis, and DNA damage, while the ash leachate was safer/more biocompatible as compared with solid ash in term of toxicity. Prabhakar et al. have investigated the marine toxicity and human cell line toxicity of raw ash and acid-treated ash. The results showed that acid-treated ash is more toxic towards marine organisms as compared with raw ash, and the raw ash particles displayed size and dose dependent toxicity against human cell lines, while the leachate proved safe even at a high L/S ratio (Prabhakar et al., 2021). This work mainly focuses on the deposition patterns of fly ash particles and analysis of heavy metal-related health risk in the human respiratory system. The risk of inhalation exposure to the selected heavy metals was estimated based on the US EPA supplemented guidance (EPA USA, 2009). Eq. (9) was applied to measure the inhalation exposure concentration for each heavy metal:

$$EC = C \times ET \times EF \times ED/ATn \quad (9)$$

Where EC (μg/m^3) is the exposure concentration. C (μg/m^3) refers to the average heavy metal concentration. ET (hours/day), EF (days/year), and ED (years) are the exposure time, frequency, and duration, respectively. For the industry scenario, ET, EF, and ED are 8 hours/day, 300 days/year, and 30 years, respectively. ATn is the average time of exposure. For non-carcinogens, ATn = ED × 365 days/year × 24 hours/day, while for carcinogens, ATn=70 years × 365 days/year × 24 hours/day.

The non-carcinogenic risk is evaluated based on the hazard quotient (HQ), which is calculated by the following equation:

$$HQ = EC/(RfC \times 1000) \quad (10)$$

where RfC (mg/m^3) is the inhalation reference concentration. The cut-off point of significant health risks is HQ=1.

The carcinogenic risk is evaluated based on the excess lifetime cancer risk (ELCR), which is calculated by the following equation:

$$ELCR = IUR \times EC \quad (11)$$

where IUR ((μg/m^3)$^{-1}$) is the inhalation unit risk. ELCR denotes the probability of developing cancer due to exposure to a specific pollutants for 70 years and its tolerance level is 1×10^{-6}. Both RfC and IUR are obtained from EPA (EPA USA, 2016).

3 Results and discussion

3.1 Fly ash characteristics

The SEM micrographs of the five fly ash samples are shown in **Fig. 2**. Type (I) fly ash particles are featured by mixed shapes (fibrous, spherical, and isometric). Type (II) particles are mainly in a spherical shape. Type (III) particles are fibres alike. Type (IV) and (V) particles have an isometric shape.

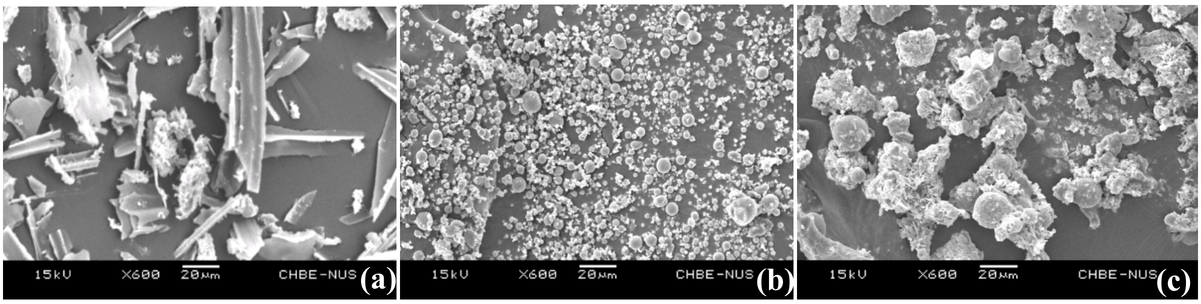

Fig. 2 The SEM micrographs of the 3 fly ash samples.

The morphology of particles has a significant effect on their transport dynamics and determines how deeply they could penetrate into the airways (Hinds, 2012). An image processing program (ImageJ) was used to estimate the characteristic length (average equivalent (circular) radius) of fly ash based on the areas occupied. Since type III particles generally have a low circularity, their characteristic length, i.e. the longest distance from edge to edge was measured instead of the equivalent radius. The specific surface area and pore size of particles are closely related to the chemical exchange between deposited particles and airway surfaces (Noël et al., 2017; Schmid and Stoeger, 2016). The physical characteristics of the fly ash samples are summarized in **Table 1.**

Table 1. Physical characteristics of fly ash samples.

Fly ash	Specific surface area (cm^2/g)	Average particle diameter (μm)	Feature
a	1128.24	19.62	Fibres
b	2880.86	7.69	Spherical
c	510.55	43.37	Isometric

3.2 Transport dynamics and fluid mechanisms

In general, particle transport and deposition in the respiratory system are attributed to three main mechanisms, i.e. sedimentation, diffusion, and impaction. Sedimentation is affected by the velocity of air flow, particle size and mass, and geometry and dimension of airways (Hofmann, 2011). Under the sedimentation mechanism, larger particles in the range of micrometers will start depositing in the airways due to gravity as the air velocity decreases down the airway generations due to pressure drop and branching. For the case of vertical orientation, the effect of sedimentation is mitigated. The diffusion mechanism is originated from the random Brownian motion of suspended particles via convective transport and thus the most effective for sub-micrometer (< 0.5 μm) particles. The fly ash particles used in this study are much larger and correspond to diffusivity constants of less than 10^{-11} m^2 s^{-1}. Hence, the diffusion is expected to play a minor role in the particle deposition. Deposition by impaction occurs frequently at branching edges and constrictions in the TB region when particles with high momentum deviate from the curved and narrowed airways and intercept with the surfaces of the airways. This is expected to be a dominant mechanism for the particles involved in this study (Hinds, 2012).

3.2.1 Deposition efficiency vs flow rate

Fig. 3 illustrate the typical deposition efficiency achieved by the three types of fly ash (a, b, and c) under different air flow rates (10L/min vs. 25L/min) but retaining the same duration of breathing cycle (inhalation + exhalation). The general trend observed in all three cases is that under the same duration of breathing cycle, the deposition efficiency at the flow rate of 10L/min is lower than that at the flow rate of 25L/min. It is expected that there is an overall reduction of deposition efficiency upon the increase of air flow rate under the scenario that sedimentation plays a dominant role in fly ash deposition. Less particles will deposit via sedimentation under higher breathing flowrate. It is also observed that in daughter tube, the high deposition efficiency greater than 60% associated with particle sizes greater than 15 microns. It is also interesting to note that in the parent tube, the deposition pattern for all the three types of ash remained relatively the same, which is different from the daughter tube. The effect may result from different deposition mechanisms. The deposition of coarse particles in the respiratory tract is mainly caused by gravitational sedimentation and impaction, while diffusion is the primary mechanism for sub-micron particles, especially for ultrafine particles. The corresponding result for the average deposition efficiency under different breathing depths is found in **Table 2**. The results show higher deposition observed in daughter tubes than the parent tubes.

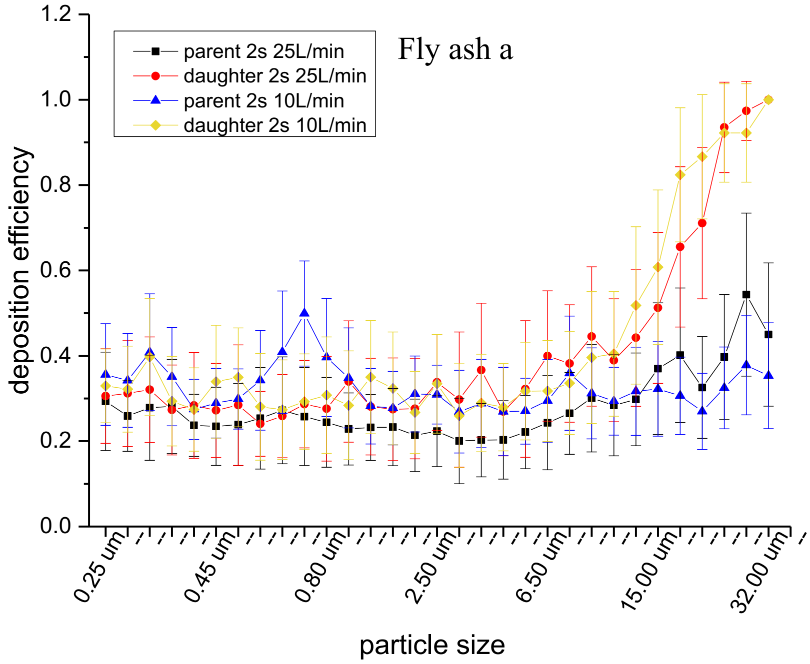
Fly ash a
parent 2s 25L/min
daughter 2s 25L/min
parent 2s 10L/min
daughter 2s 10L/min
deposition efficiency
particle size
0.0
0.2
0.4
0.6
0.8
1.0
1.2
0.25 um
0.45 um
0.80 um
2.50 um
6.50 um
15.00 um
32.00 um

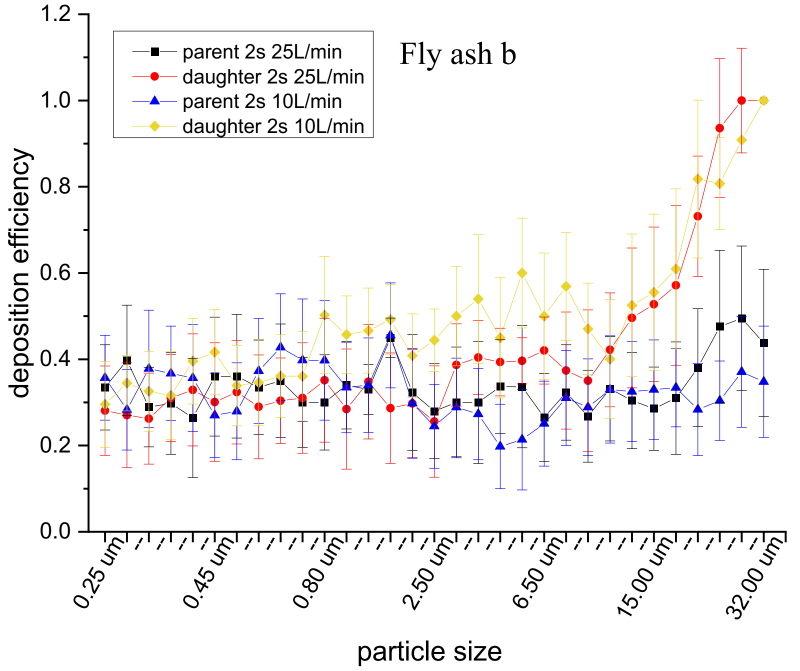
Fly ash b
parent 2s 25L/min
daughter 2s 25L/min
parent 2s 10L/min
daughter 2s 10L/min
deposition efficiency
particle size
0.0
0.2
0.4
0.6
0.8
1.0
1.2
0.25 um
0.45 um
0.80 um
2.50 um
6.50 um
15.00 um
32.00 um

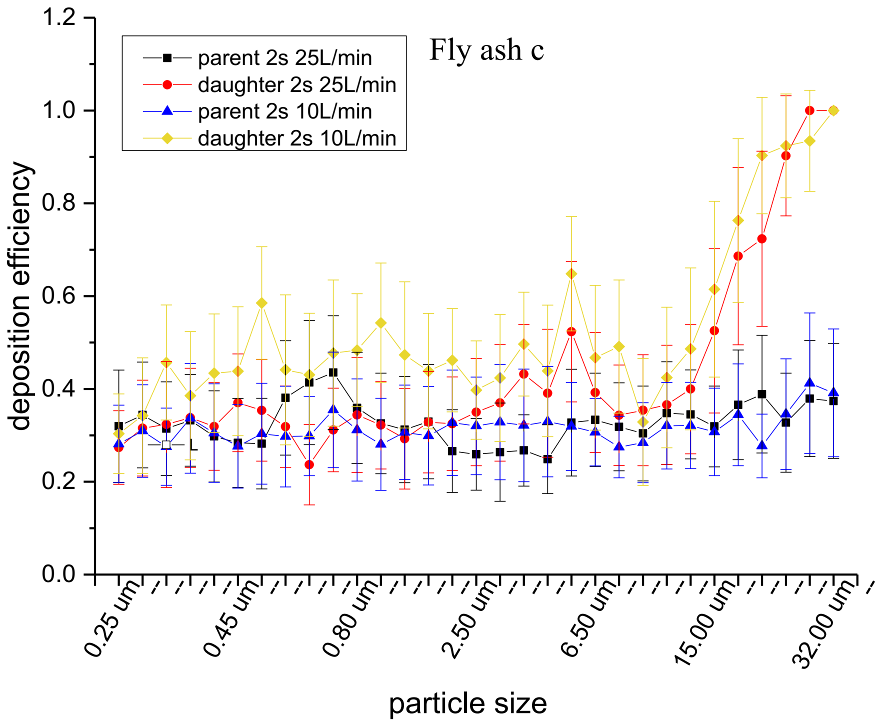

Fig. 3 Deposition efficiency vs flow rate for three types of fly ash. The duration of one cycle of experiment (inhalation + exhalation) is 2s.

3.2.2 Deposition efficiency vs breathing frequency

Fig. 4 illustrates the dependence of deposition efficiency and breathing frequency. It is observed that with flow rate increasing from 10L/min to 25L/min, (breathing frequency 30 times/min), average particle deposition efficiency (The value 1 corresponds to 100% deposition) in parent tube decreases from 0.33 to 0.28, 0.34 to 0.32, and 0.33 to 0.32 respectively, for ashes a, b and c. Average particle deposition efficiency in daughter tube decreases from 0.43 to 0.41, 0.52 to 0.47, and 0.44 to 0.43 respectively, for ashes a, b and c.

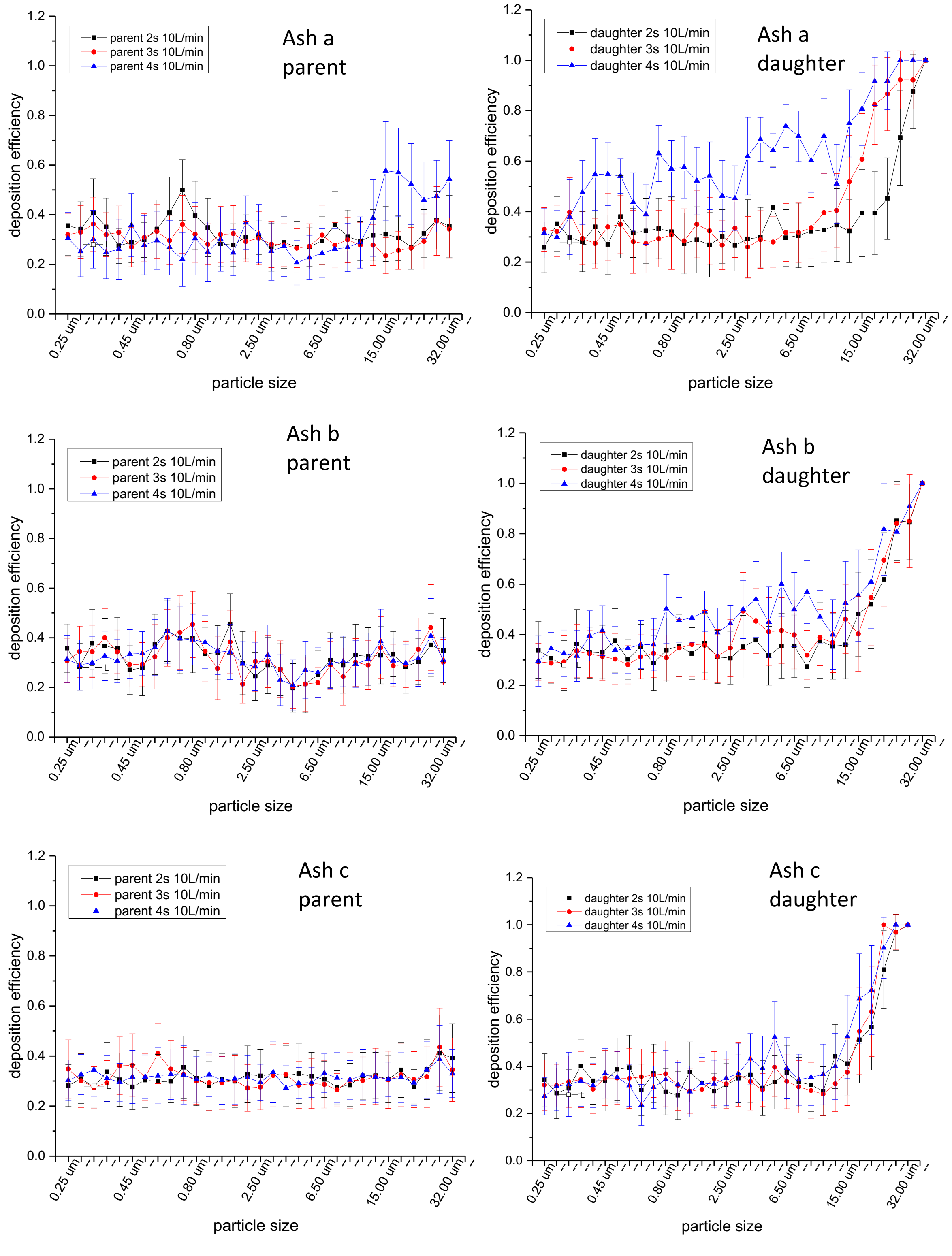

Fig. 4 Deposition efficiency vs. breathing frequency.

In contrast, with breathing frequency decreasing from 30 times/min to 20 times/min (10 L/min flowrate), average particle deposition efficiency in parent tube increases from 0.33 to 0.37, 0.34 to 0.40, and 0.33 to 0.38 respectively, for ashes a, b and c. Average particle deposition efficiency in daughter tube increases from 0.43 to 0.61, 0.52 to 0.60, and 0.44 to 0.45 respectively, for ashes a, b and c.

Particle size has strong impact on the particle deposition efficiency in the daughter tube. There is a significant increase of deposition efficiency with increasing particle size. Based on the data sets presented, micro-particle tends to deposit deeply in daughter tube. The branching results in the reduction of air flow rate so that heavy and large fly ash particles could not be transported deeper into the bifurcation tube. The inertial of airborne particles were greater at higher flow rates and more fly ash particles were expected to deviate and deposit at the daughter tubes. **Table 2** summarizes the average deposition efficiency under different physiological conditions simulated by modulating the duration of breathing cycle as 2s, 3s, 4s, respectively. While ash a, b and c exhibit similar deposition profiles in the parent tube and daughter tube, it is observed that the average deposition efficiency is in the order of c>a>b. This is determined by the combined effects of particle morphology, particle surface area and average particle size.

Table 2. Average deposition efficiency under different physiological conditions simulated by modulating inhalation + exhalation cycle as 2s, 3s, 4s, respectively. P: Parent tube. D: Daughter tube.

		10L/min 2s		**25L/min 2s**		**10L/min 3s**		**25L/min 3s**		**10L/min 4s**		**25L/min 4s**	
		P	D	P	D	P	D	P	D	P	D	P	D
Fly ash a	DE	0.44	0.63	0.40	0.61	0.48	0.69	0.44	0.67	0.52	0.74	0.47	0.72
Fly ash b	DE	0.34	0.52	0.32	0.47	0.37	0.57	0.35	0.52	0.4	0.61	0.38	0.55
Fly ash c	DE	0.63	0.68	0.58	0.65	0.69	0.75	0.64	0.72	0.74	0.8	0.68	0.76

3.3 Health risk assessment

The heavy metal concentration of three ashes are listed in **Table 3**. The heavy metals in **Table 3** were selected according to our group's previous research work (Lin et al., 2018). There is no heavy metal detectable in fly ash b as it is generated from burning of biomass sawdust. Fly ash a and fly ash c is generated from industrial boiler and combustion of sewage sludge, respectively. With regard to the calculation of HQ, only As (RfC = 0.00003 mg/m^3) and Cr (RfC = 0.000008 mg/m^3) are selected for the evaluation of non- carcinogenic risk, because EPA (IRIS 2006) has not recommended an inhalation reference concentration (RfC) for Ba, Cu, Pb, and Zn. The acceptable risk limits for HQ and ELCR are 1 and 1 × 10^{-6}, respectively.

Table 3. Heavy metal concentrations.

Element (g/kg)	Fly ash a (from combustion of coal)	Fly ash c (from combustion of sewage sludge)
As	0.04	ND
Ba	0.11	0.07
Cd	ND	ND
Co	ND	ND
Cr	0.05	0.07
Cu	0.08	0.19
Hg	ND	0.16
Mn	1.54	0.33
Mo	ND	ND
Ni	ND	0.06
Pb	0.13	ND
Sb	ND	ND
Se	ND	ND
Zn	1.03	0.4

Non-carcinogenic risk and carcinogenic risk of selected heavy metal elements are listed in **Table 4** and **Table 5**, respectively. In general, non-carcinogenic risk and carcinogenic risk of selected heavy metal elements are directly proportional to their deposition efficiency in the simulated human respiratory system. Both non-carcinogenic risk and carcinogenic risk are in negative correlation with breathing frequency and flow rate. In addition, the HRA results show that most of the heavy metal elements have the non-carcinogenic risk being within the accepted limit (HQ = 1). Cr and Mn pose a potential non-carcinogenic risk in deposition scenarios of fly ash a and c. The non-carcinogenic risk of Mn in the exposure scenario of fly ash a is approaching the acceptable limit because fly ash a contains significantly higher amount of Mn than fly ash c. Cr poses the highest carcinogenic risk in the exposure scenario of fly ash c. Both As and Cr may pose a potential carcinogenic risk for people who are involved with the exposure scenario of fly ash a (i.e. people who are working in the industrial boiler plants). Apart from the heavy metals, polycyclic aromatic hydrocarbons (PAHs) are another group of toxic compounds which pose severe risks to human health. PAHs are formed during the incomplete combustion of hydrocarbon compounds. The gas phase of PAHs will get cooled once it leaves the high-temperature flame, and get deposited in the solid ash phase through nucleation, condensation, or adsorption (Megido et al., 2016). The concentration of various PAHs in fly ash and their corresponding toxicity to human health will be investigated using the similar method for our future work.

Table 4. Hazard quotient of ash a and c.
(PM mass concentration in industrial area is 42 ug/m^3)

		10L/min 2s	25L/min 2s	10L/min 3s	25L/min 3s	10L/min 4s	25L/min 4s
ash a	Cr	4.56×10^{-3}	4.41×10^{-3}	4.83×10^{-3}	4.69×10^{-3}	5.04×10^{-3}	4.9×10^{-3}
	Mn	2.81×10^{-1}	2.71×10^{-1}	2.97×10^{-1}	2.89×10^{-1}	3.10×10^{-1}	3.02×10^{-1}
ash c	Cr	7.10×10^{-3}	6.87×10^{-3}	7.43×10^{-3}	7.24×10^{-3}	7.64×10^{-3}	7.44×10^{-3}
	Hg	5.41×10^{-3}	5.24×10^{-3}	5.66×10^{-3}	5.52×10^{-3}	5.82×10^{-3}	5.67×10^{-3}
	Mn	6.70×10^{-2}	6.48×10^{-2}	7.01×10^{-2}	6.83×10^{-2}	7.20×10^{-2}	7.01×10^{-2}

Table 5. ELCR of ash a and c.
(PM mass concentration in industrial area is 42 ug/m^3)

		10L/min 2s	25L/min 2s	10L/min 3s	25L/min 3s	10L/min 4s	25L/min 4s

	As	6.72×10^{-7}	6.50×10^{-7}	7.11×10^{-7}	6.91×10^{-7}	7.42×10^{-7}	7.22×10^{-7}
ash a	Cr	2.35×10^{-6}	2.27×10^{-6}	2.48×10^{-6}	2.41×10^{-6}	2.59×10^{-6}	2.52×10^{-6}
	Pb	6.10×10^{-9}	5.89×10^{-9}	6.45×10^{-9}	6.27×10^{-9}	6.73×10^{-9}	6.55×10^{-9}
ash c	Cr	3.65×10^{-6}	3.53×10^{-6}	3.82×10^{-6}	3.72×10^{-6}	3.93×10^{-6}	3.82×10^{-6}
	Ni	6.26×10^{-8}	6.06×10^{-8}	6.55×10^{-8}	6.39×10^{-8}	6.73×10^{-8}	6.56×10^{-8}

3.4 Deposition percentage of respiratory particles containing SARS-CoV-2

In this study, respiratory particles with three representative sizes, i.e., 0.4um, 1.9um, and 9um, have been chosen to simulate the deposition of respiratory particles to which SARS-CoV-2 is attached (Lee, 2020b). **Table 6** shows the DP in parent and daughter tubes of respiratory particles with different sizes under different physiological conditions simulated by modulating respiratory cycle as 2s, 3s, 4s, respectively. It is observed that DP in the parent tube is higher than that in the daughter tube in most scenarios, which indicates that more SARS-CoV-2 deposits in the upper extrathoracic airways compared with the lower bronchi airway. The size of RP does not affect their DP in both parent or daughter tubes. However, the larger the RP is, the fewer virus the RP contains. This will further affect the total amount of viruses deposited in human airways (Lee, 2020a). Although there is no significant difference of DP under different respiratory cycles, it is noted that when the breath rate increases from 10 L/ min to 25 L/ min, the DP in both parent and daughter tubes decrease in most scenarios.

Table 6. Average deposition percentage in parent and daughter tubes of respiratory particles with different sizes under different physiological conditions simulated by modulating breathing cycle as 2s, 3s, 4s, respectively. P: Parent tube. D: Daughter tube.

	10L/min 2s		**25L/min 2s**		**10L/min 3s**		**25L/min 3s**		**10L/min 4s**		**25L/min 4s**	
	P	D	P	D	P	D	P	D	P	D	P	D
RP-0.4um	0.357	0.254	0.264	0.242	0.343	0.213	0.315	0.216	0.307	0.274	0.277	0.278
RP-1.9um	0.298	0.287	0.323	0.201	0.213	0.248	0.202	0.229	0.295	0.288	0.280	0.265
RP-9um	0.330	0.268	0.332	0.282	0.301	0.258	0.279	0.255	0.294	0.283	0.270	0.278

4 Conclusions

In this work, we conducted a series of fly ash transport and deposition experiments in a bifurcation airway model using optical aerosol sampling analysis. It is found that breathing flow rate, breathing frequency, and particle size play important role in particle transport and deposition in the human respiratory system. Deposition efficiency of respiratory particles decreases with increasing breathing flow rate and increasing breathing frequency. Micro-particle tends to deposit deeply in daughter tube. It is also noted that deposition percentage in the parent tube is higher than that in the daughter tube, which indicates that more SARS-CoV-2 deposits in the upper extrathoracic airways compared with the lower bronchi airway. This study could fulfil the gap of imbalance between the advancement of computational methods and experimental study on less ideal non-spherical dust particles. The results could potentially serve as a basis for setting health guidelines and recommending personal respiratory protective equipment for on-site employees who are in the high exposure risk environment of fly ash and COVID-19 virus.

ACKNOWLEDGEMENT

The authors acknowledge the funding support from the National Research Foundation (NRF), Prime Minister's Office, Singapore under its Campus for Research Excellence and Technological Enterprise (CREATE) program. Grant Number A0001032-01-00, National University of Singapore.

References

.

Aykac, D., Hoffman, E.A., McLennan, G., Reinhardt, J.M., 2003. Segmentation and analysis of the human airway tree from three-dimensional X-ray CT images. IEEE Transactions on Medical Imaging 22, 940-950.

Banko, A., Coletti, F., Schiavazzi, D., Elkins, C., Eaton, J., 2015. Three-dimensional inspiratory flow in the upper and central human airways. Experiments in Fluids 56, 117.

Bao, L.M., Zhang, G.L., Lei, Q.T., Li, Y., Li, X.L., Hwu, Y.K., Yi, J.M., 2015. Microstructure of atmospheric particles revealed by TXM and a new mode of influenza virus transmission. Nucl Instrum Methods Phys Res B 359, 167-172.

Bharadvaj, B., Mabon, R., Giddens, D., 1982. Steady flow in a model of the human carotid bifurcation. Part I-flow visualization. Journal of Biomechanics 15, 349-362.

Carvalho, G.M.C., da Silva Nagato, L.K., da Silva Fagundes, S., dos Santos, F.B., Calheiros, A.S., Malm, O., Bozza, P.T., Saldiva, P.H.N., Faffe, D.S., Rocco, P.R.M., 2014. Time course of pulmonary burden in mice exposed to residual oil fly ash. Frontiers in Physiology 5.

Conticini, E., Frediani, B., Caro, D., 2020. Can atmospheric pollution be considered a co-factor in extremely high level of SARS-CoV-2 lethality in Northern Italy? Environ Pollut 261, 114465.

Coronaviridae Study Group of the International Committee on Taxonomy of, V., 2020. The species Severe acute respiratory syndrome-related coronavirus: classifying 2019-nCoV and naming it SARS-CoV-2. Nat Microbiol 5, 536-544.

Dwivedi, S., Saquib, Q., Al-Khedhairy, A.A., Ali, A.-Y.S., Musarrat, J., 2012. Characterization of coal fly ash nanoparticles and induced oxidative DNA damage in human peripheral blood mononuclear cells. Science of The Total Environment 437, 331-338.

EPA USA, 2009. Risk Assessment Guidance for Superfund Volume I: Human Health Evaluation Manual (Part F, Supplemental Guidance for Inhalation Risk Assessment).

EPA USA, 2016. Regional Screening Levels (RSLs) - Generic Tables (May 2016).

Fang, T., Zeng, L., Gao, D., Verma, V., Stefaniak, A.B., Weber, R.J., 2017. Ambient size distributions and lung deposition of aerosol Dithiothreitol-measured oxidative potential: A contrast between soluble and insoluble particles. Environmental Science & Technology.

Feng, Y., Kleinstreuer, C., 2014. Micron-particle transport, interactions and deposition in triple lung-airway bifurcations using a novel modeling approach. Journal of Aerosol Science 71, 1-15.

Goikoetxea, E., Murgia, X., Serna-Grande, P., Valls-i-Soler, A., Rey-Santano, C., Rivas, A., Antón, R., Basterretxea, F.J., Miñambres, L., Méndez, E., 2014. In vitro surfactant and perfluorocarbon aerosol deposition in a neonatal physical model of the upper conducting airways. PloS One 9, e106835.

Hidy, G., 2012. Aerosols: an industrial and environmental science. Elsevier.

Hinds, W.C., 2012. Aerosol technology: properties, behavior, and measurement of airborne particles. John Wiley & Sons.

Hofmann, W., 2011. Modelling inhaled particle deposition in the human lung-A review. Journal of Aerosol Science 42, 693-724.

Hong, J.L.X., Maneerung, T., Koh, S.N., Kawi, S., Wang, C.-H., 2017. Conversion of coal fly ash into zeolite materials: synthesis and characterizations, process design, and its cost-benefit analysis. Industrial & Engineering Chemistry Research 56, 11565-11574.

Islam, M.S., Larpruenrudee, P., Paul, A.R., Paul, G., Gemci, T., Gu, Y., Saha, S.C., 2021. SARS CoV-2 aerosol: How far it can travel to the lower airways? Phys Fluids (1994) 33, 061903.

J. Marvin Herndon, M.W., 2020. Aerosol Particulates, SARS-CoV-2, and the Broader Potential for Global Devastation. Journal of Internal Medicine 3, 14-21.

Jayaweera, M., Perera, H., Gunawardana, B., Manatunge, J., 2020. Transmission of COVID-19 virus by droplets and aerosols: A critical review on the unresolved dichotomy. Environ Res 188, 109819.

Jedelsky, J., Lizal, F., Jicha, M., 2012. Characteristics of turbulent particle transport in human airways under steady and cyclic flows. International Journal of Heat and Fluid Flow 35, 84-92.

Johnson, D.R., 2016. Nanometer-sized emissions from municipal waste incinerators: A qualitative risk assessment. Journal of Hazardous Materials 320, 67-79.

Kerekes, A., Nagy, A., Veres, M., Rigó, I., Farkas, Á., Czitrovszky, A., 2016. In vitro and in silico (IVIS) flow characterization in an idealized human airway geometry using laser Doppler anemometry and computational fluid dynamics techniques. Measurement 90, 144-150.

Kim, C.S., Fisher, D.M., 1999. Deposition characteristics of aerosol particles in sequentially bifurcating airway models. Aerosol Science & Technology 31, 198-220.

Kolanjiyil, A.V., Kleinstreuer, C., 2016. Computationally efficient analysis of particle transport and deposition in a human whole-lung-airway model. Part I: Theory and model validation. Computers in Biology and Medicine 79, 193-204.

Lee, B.U., 2020a. Minimum Sizes of Respiratory Particles Carrying SARS-CoV-2 and the Possibility of Aerosol Generation. Int J Environ Res Public Health 17.

Lee, B.U., 2020b. Minimum sizes of respiratory particles carrying SARS-CoV-2 and the possibility of aerosol generation. International journal of environmental research and public health 17, 6960.

Lee, J., Yoo, D., Ryu, S., Ham, S., Lee, K., Yeo, M., Min, K., Yoon, C., 2019. Quantity, Size Distribution, and Characteristics of Cough-generated Aerosol Produced by Patients with an Upper Respiratory Tract Infection. Aerosol and Air Quality Research 19, 840-853.

Li, B., Deng, Z., Wang, W., Fang, H., Zhou, H., Deng, F., Huang, L., Li, H., 2017. Degradation characteristics of dioxin in the fly ash by washing and ball-milling treatment. Journal of Hazardous Materials.

Lin, W.Y., Ng, W.C., Wong, B.S.E., Teo, S.L.-M., Baeg, G.H., Ok, Y.S., Wang, C.-H., 2018. Evaluation of sewage sludge incineration ash as a potential land reclamation material. Journal of hazardous materials 357, 63-72.

Madas, B.G., Furi, P., Farkas, A., Nagy, A., Czitrovszky, A., Balashazy, I., Schay, G.G., Horvath, A., 2020. Deposition distribution of the new coronavirus (SARS-CoV-2) in the human airways upon exposure to cough-generated droplets and aerosol particles. Sci Rep 10, 22430.

Marchini, T., Magnani, N.D., Paz, M.L., Vanasco, V., Tasat, D., Maglio, D.G., Alvarez, S., Evelson, P.A., 2014. Time course of systemic oxidative stress and inflammatory response induced by an acute exposure to residual oil fly ash. Toxicology and Applied Pharmacology 274, 274-282.

Mason, R.J., 2020. Pathogenesis of COVID-19 from a cell biology perspective. Eur Respir J 55.

Matzenbacher, C.A., Garcia, A.L.H., dos Santos, M.S., Nicolau, C.C., Premoli, S., Corrêa, D.S., de Souza, C.T., Niekraszewicz, L., Dias, J.F., Delgado, T.V., 2017. DNA damage induced by coal dust, fly and bottom ash from coal combustion evaluated using the micronucleus test and comet assay in vitro. Journal of Hazardous Materials 324, 781-788.

Megido, L., Suárez-Peña, B., Negral, L., Castrillón, L., Suárez, S., Fernández-Nava, Y., Marañón, E., 2016. Relationship between physico-chemical characteristics and potential toxicity of PM_{10}. Chemosphere 162, 73-79.

Mozhi, A., Prabhakar, A.K., Mohan, B.C., Sunil, V., Teoh, J.H., Wang, C.-H., 2022. Toxicity effects of size fractions of incinerated sewage sludge bottom ash on human cell lines. Environment International 158, 106881.

Noël, A., Truchon, G., Cloutier, Y., Charbonneau, M., Maghni, K., Tardif, R., 2017. Mass or total surface area with aerosol size distribution as exposure metrics for inflammatory, cytotoxic and oxidative lung responses in rats exposed to titanium dioxide nanoparticles. Toxicology and Industrial Health 33, 351-364.

Nyale, S.M., Babajide, O.O., Birch, G.D., Böke, N., Petrik, L.F., 2013. Synthesis and characterization of coal fly ash-based foamed geopolymer. Procedia Environmental Sciences 18, 722-730.

Oliveira, M.L., Navarro, O.G., Crissien, T.J., Tutikian, B.F., da Boit, K., Teixeira, E.C., Cabello, J.J., Agudelo-Castañeda, D.M., Silva, L.F., 2017. Coal emissions adverse human health effects associated with ultrafine/nano-particles role and resultant engineering controls. Environmental Research 158, 450-455.

Park, S., Wexler, A., 2008. Size-dependent deposition of particles in the human lung at steady-state breathing. Journal of Aerosol Science 39, 266-276.

Peslin, R., Fredberg, J.J., 2011. Oscillation mechanics of the respiratory system. Comprehensive Physiology.

Pleil, J.D., Ariel Geer Wallace, M., Davis, M.D., Matty, C.M., 2021. The physics of human breathing: flow, timing, volume, and pressure parameters for normal, on-demand, and ventilator respiration. J Breath Res 15.

Prabhakar, A.K., Mohan, B.C., Tay, T.S., Lee, S.S.-C., Teo, S.L.-M., Wang, C.-H., 2021. Incinerated sewage sludge bottom ash-chemical processing, leaching patterns and toxicity testing. Journal of Hazardous Materials 402, 123350.

Rahimi-Gorji, M., Gorji, T.B., Gorji-Bandpy, M., 2016. Details of regional particle deposition and airflow structures in a realistic model of human tracheobronchial airways: Two-phase flow simulation. Computers in Biology and Medicine 74, 1-17.

Sankhala, S., Singh, H.S., Singh, S.K., Lalwani, G., 2013. Factors That Affect the Lung Deposition. International Journal of Modern Physics: Conference Series 22, 729-732.

Santa, R.A.A.B., Soares, C., Riella, H.G., 2016. Geopolymers with a high percentage of bottom ash for solidification/immobilization of different toxic metals. Journal of Hazardous Materials 318, 145-153.

Schmid, O., Stoeger, T., 2016. Surface area is the biologically most effective dose metric for acute nanoparticle toxicity in the lung. Journal of Aerosol Science 99, 133-143.

Sgro, L.A., D'Anna, A., Minutolo, P., 2012. On the characterization of nanoparticles emitted from combustion sources related to understanding their effects on health and climate. Journal of Hazardous Materials 211, 420-426.

Shaik, Z., Ramulu, V., Hanimann, K., 2017. A study on anatomical dimensions of bronchial tree. International Journal of Research in Medical Sciences 4, 2761-2765.

Shanley, K.T., Ahmadi, G., Hopke, P.K., Cheng, Y.-S., 2016. Simulated airflow and rigid fiber behavior in a realistic nasal airway model. Particulate Science and Technology, 1-10.

Subbarao, K., Mahanty, S., 2020. Respiratory Virus Infections: Understanding COVID-19. Immunity 52, 905-909.

Terzić, A., Pavlović, L., Radojević, Z., Pavlović, V., Mitić, V., 2015. Novel utilization of fly ash for high-temperature mortars: Phase composition, microstructure and performances correlation. International Journal of Applied Ceramic Technology 12, 133-146.

Theunissen, R., Riethmuller, M.L., 2007. Particle image velocimetry in lung bifurcation models, Particle Image Velocimetry. Springer, pp. 73-101.

Tong, X., Dong, J., Shang, Y., Inthavong, K., Tu, J., 2016. Effects of nasal drug delivery device and its orientation on sprayed particle deposition in a realistic human nasal cavity. Computers in Biology and Medicine 77, 40-48.

Wedel, J., Steinmann, P., Strakl, M., Hribersek, M., Ravnik, J., 2021. Can CFD establish a connection to a milder COVID-19 disease in younger people? Aerosol deposition in lungs of different age groups based on Lagrangian particle tracking in turbulent flow. Comput Mech, 1-17.

worldometer, 2022. COVID-19 CORONAVIRUS PANDEMIC.

Wu, S., Zhou, J., Pan, Y., Zhang, J., Zhang, L., Ohtsuka, N., Motegi, M., Yonemochi, S., Oh, K., Hosono, S., 2016. Dioxin distribution characteristics and health risk assessment in different size particles of fly ash from MSWIs in China. Waste Management 50, 113-120.

Xu, Q., Leong, F.Y., Wang, C.-H., 2009. Transport and deposition of inertial aerosols in bifurcated tubes under oscillatory flow. Chemical Engineering Science 64, 830-846.

Yao, H., Song, Y., Chen, Y., Wu, N., Xu, J., Sun, C., Zhang, J., Weng, T., Zhang, Z., Wu, Z., Cheng, L., Shi, D., Lu, X., Lei, J., Crispin, M., Shi, Y., Li, L., Li, S., 2020. Molecular Architecture of the SARS-CoV-2 Virus. Cell 183, 730-738 e713.

You, S., Yao, Z., Dai, Y., Wang, C.-H., 2017. A comparison of PM exposure related to emission hotspots in a hot and humid urban environment: Concentrations, compositions, respiratory deposition, and potential health risks. Science of The Total Environment 599, 464-473.

Zamankhan, P., Ahmadi, G., Wang, Z., Hopke, P.K., Cheng, Y.-S., Su, W.C., Leonard, D., 2006. Airflow and deposition of nano-particles in a human nasal cavity. Aerosol Science and Technology 40, 463-476.

Zhang, Y., Zhao, B., Li, X., 2006. Perceived particle intensity: an indicator to evaluate indoor particle pollution. Indoor and Built Environment 15, 155-164.